PNAS
www.pnas.org

Supplementary Information for

Cellular hysteresis as a principle to maximize the efficacy of antibiotic therapy

Roderich Roemhild, Chaitanya S. Gokhale, Philipp Dirksen, Christopher Blake, Philip Rosenstiel, Arne Traulsen, Dan I. Andersson, Hinrich Schulenburg

Hinrich Schulenburg
Email: hschulenburg@evolbio.mpg.de

This PDF file includes:

SI Materials and Methods
Figs. S1 to S11
Tables S1 to S7
Captions for movies S1 to S1
Captions for datasets S1 to S5
References for SI reference citations

Other supplementary materials for this manuscript include the following:

Movies S1 to S1
Datasets S1 to S5

www.pnas.org/cgi/doi/10.1073/pnas.1810004115

SI Materials and Methods

Main evolution experiment. We performed parallel experimental evolution in 16 different treatment protocols of the bactericidal antibiotics CIP (Sigma-Aldrich, USA; Ref. 17850-5G-F), GEN (Carl Roth, Germany; Ref. HN09.1), and CAR (Carl Roth, Germany; Ref. 6344.2). We generated three regular sequences starting with different antibiotics and in two switching rates, yielding sequences ##5 -7 with switches every 12 h and ##8-10 with switches every 48h. Six sequences with random order, ##11-16, were generated from atmospheric noise (random.org, Randomness and Integrity Services Ltd., Ireland) and rotated to obtain two sequences each starting either with CIP, GEN or CAR. The 12 replicates per treatment protocol were founded by $5x10^5$ exponential phase cells from six independent PA14 starting cultures. Antibiotics concentrations were standardized to IC_{75} and concentrations were constant for the whole experiment (CIP 40 ng/ml, GEN 480 ng/ml, CAR 50 µg/ml). The experiment was performed in 96-well plates (Greiner Bio-One, Germany; Ref. 655161) that were incubated in plate readers (BioTek Instruments, USA; Ref. EON) with 180rpm double orbital shaking at 37°C for 96 transfers of 12 h during which we measured OD_{600} every 15 min. Incubation for 12 h was sufficient for adapted bacteria to reach carrying capacity, in which case they would grow 5.6 generations between transfers. Evolved material was conserved every 12 transfers by freezing to -80°C in 10% (vol/vol) DMSO.

Quantification of cumulative hysteresis levels and switching irregularity. To quantify the experienced hysteresis levels, we multiplied occurrences of the six different drug switches up to a particular time point with their respective hysteresis values, from which the sum of products was calculated and normalized by dividing by the number of transfers up to that time point. Switching irregularity *IR* was quantified using a modified entropy index. For a defined time window and drug proportions p_i, $IR = (|p_{CIP}*\log_2(p_{CIP}) - p_{GEN}*\log_2(p_{GEN})| + |p_{CIP}*\log_2(p_{CIP}) - p_{CAR}*\log_2(p_{CAR})| + |p_{GEN}*\log_2(p_{GEN}) - p_{CAR}*\log_2(p_{CAR})|)/3$.

Identification of subpopulations. Subpopulations were identified by hierarchical clustering of the resistance profiles of isolates from the same population and time point with the *R* package *pvclust* (https://cran.r-project.org/web/packages/pvclust/index.html): method = *average*, *euclidean* distances. Different clustering algorithms (*median*, *ward.D2*) yielded the same clusters. This analysis identified groups of isolates that share dose-responses that are correlated between antibiotics. Isolates were added to a new cluster if they had a height larger than the threshold of $h = 0.2$. After applying clustering with this threshold, the residual variation in dose-response curves was lower than that of the isogenic strain PA14. Cluster frequencies were used to calculate within-population diversity using Shannon entropy.

Growth rate measurements of evolved isolates. Maximum exponential growth rates of evolved isolates were calculated from growth curves in drug-free media and OD_{600} measurements every 15 min. The growth rate *k* was calculated in sliding windows of 0.5 h, yielding hill-shaped curves with two peaks: the first peak for growth on glucose and the second for growth on citrate (SI Appendix, Fig. S4). The reported growth rates are the maximum values of the first, larger peak.

Genomics. Genomic DNA was isolated using an established protocol (1). Resistance profiles of the cultures were verified in parallel (SI Appendix, Fig. S3). Sequencing was performed using the Illumina MiSeq 2x150bp paired-end technology and Nextera XT library preparation (Institute of Clinical Molecular Biology, Kiel, Germany). Paired reads were filtered with *Trimmomatic* (2) and mapped to the UCBPP_PA14 reference genome (3) with *Bowtie2* (4). Variants were called

using *SAMtools* (5) and filtered by *Vcftools* (MinQ = 40)(6). We subtracted mutations already present in our previously sequenced lab strain (7). Mutated intergenic regions were analysed for promoter motifs using PePPER (8). Intergenic mutations outside of promoter regions were excluded from analyses. Samples shared mutations in the genes PA14_61200 and PA14_38000, both annotated 'hypothetical protein', which were excluded from analyses.

Genetic manipulation. The *cpxS* mutation 1977519T>G (cpxS p.T163P, as selected by sequence #7) and the *mexR* mutation 486113T>T (mexR p.T130P, as selected by sequence #10) were individually introduced into the genetic background of the ancestral strain using a scar-free recombination method (9). Genetic manipulation was performed by BioVersys AG (Hochbergerstrasse 60c, CH-4057 Basel, Switzerland).

Annotation of gene *PA3206* (*PA14_22730*) as a new two-component sensor *cpxS*. Mutations in the previously uncharacterized gene PA3206 (PA14_22730) were indicated to contribute centrally to the evolutionary response to negative hysteresis. Therefore, we sought to obtain a more detailed understanding of the function of this gene. We started by analysing its genomic context in *Pseudomonas aeruginosa*. *PA3206* is in close proximity to *cpxR* (PA3204) and *cpxP* (PA3205). CpxR forms a two-component regulatory system with the sensor CpxA that is negatively regulated by CpxP in *Escherichia coli*. The genomic location suggested that *PA3206* may be a homolog of *cpxA*. However, sequence identity between CpxA from *E. coli* MG1655 (NCBI Gene [uid] 948405) and *PA3206* from PA14 was only 30%. We BLASTED the protein sequence of CpxA from MG1655 against all proteins in the NCBI database from *P. aeruginosa*. Alignments only started at residue 160, indicating differences in the N-terminal sensor domain. Indeed, the best hits were ParS, a different two-component sensor, suggesting that PA3206 is distinct from CpxA. This was confirmed by *phmmmer* analysis (aligning CpxA from MG1655 with *P. aeruginosa* proteins; https://www.ebi.ac.uk/Tools/hmmer/search/phmmer): the N-terminal periplasmic sensor domain has different structure, and also differs with respect to length, the number of transmembrane domains and the presence of a signal peptide. This line of evidence was further confirmed by a phylogenetic sequence comparison of *PA3206* with all genes that were annotated *cpxA* in the NCBI Gene database (search "cpxA[sym]") using *clustal-omega* (https://www.ebi.ac.uk/Tools/msa/clustalo/) and the closely related two-component sensor EnvZ as outgroup. We conclude that *PA3206* is a new gene, which we here name *cpxS*. We decided to keep the base-name due to its genomic context. The "*S*" denotes that it is the sensor-component of a putative envelope stress-system CpxS-CpxR in *P. aeruginosa*. The *de-novo* mutations in this study targeted the putative periplasmic sensor domain, which showed very little resemblance to the canonical sensor *cpxA* in *E. coli*, *Salmonella enterica*, *Yersinia pestis* and *P. fluorescens*, possibly indicating a currently unknown sensor function.

Measurements of hysteresis in strains resistant to the ppretreatment antibiotic. We tested whether CAR->GEN negative hysteresis can be induced in strains resistant to CAR, due to overexpression of the multidrug-efflux system MexAB-OprM. The resistant strains carried a single mutation in one of the negative regulators of the pump (*mexR* p.T130P, *nalC* deletion 1391016-1391574 (7), *nalD* p.T11N) or a mutations in the promotor region (486683C>T, as selected by sequence #3 from our evolution experiment) of the *mexAB* operon. We performed standard time-kill experiments with 600 ng/ml GEN, and with or without pretreatments with CAR for 30 min. For each strain, two pretreatment concentrations were evaluated: 200 µg/ml and their respective IC_{90} (ranging up to 600 µg/ml). As the CAR IC_{90} of the mexA strain was also 200 µg/ml, we instead tested 300 µg/ml in one of the treatments. Survival was measured after 6 h by CFU counting.

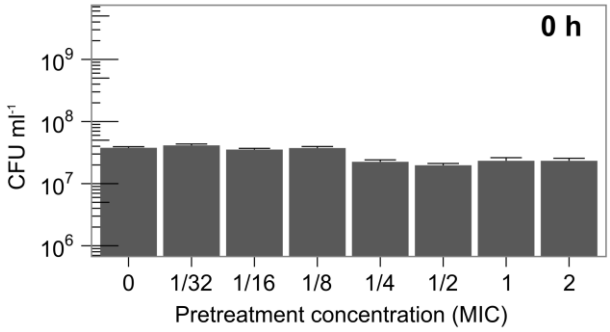

Fig. S1. Pretreatment is non-lethal. Concentration of colony forming units (CFU) of pretreated and control populations at 0 h time point, i.e. at end of the CAR pretreatment. Corresponding data for the 6 h time point is shown in Figure 1*D*. Mean ± SEM, $n = 6$.

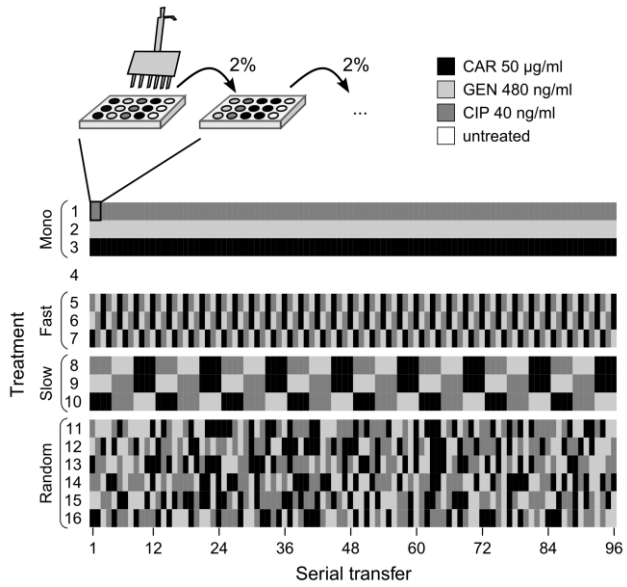

Fig. S2. Schematic of main evolution experiment with 96 serial transfers. The first 12 transfers are shown in higher magnification in Figure 2 of the main text.

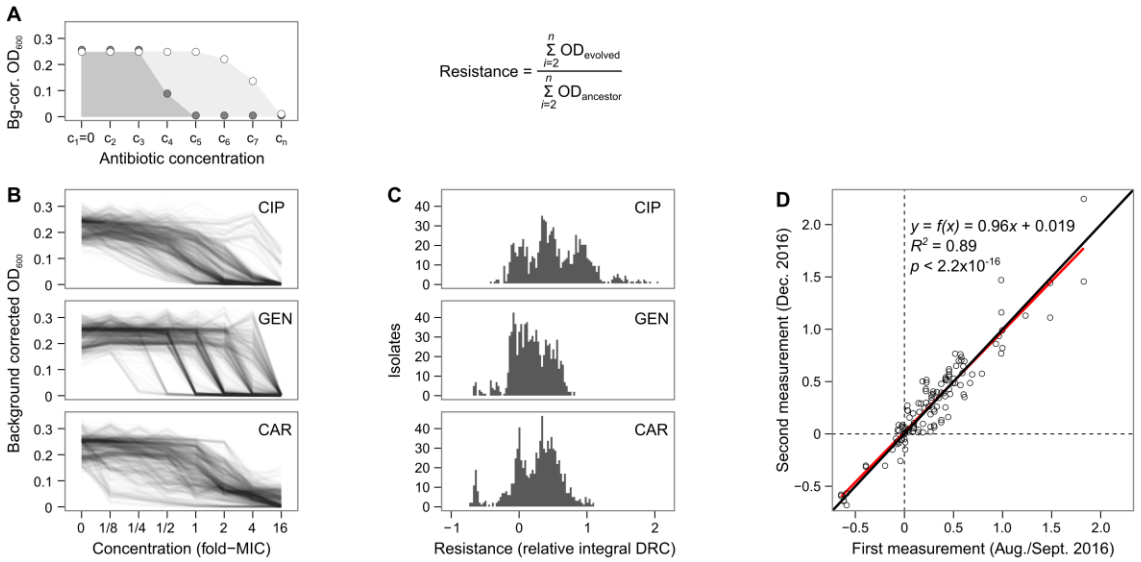

Fig. S3. Resistance measurements. (*A*) Schematic of dose-response curve (DRC) of ancestral (dark) and evolved bacteria (light) and definition of a quantitative relative resistance score based on the integral of the DRC. (*B*) DRCs of 880 evolved isolates. (*C*) Distribution of resistance scores, as defined in panel *A*, for the 880 isolates. Values lower than zero indicate hypersensitivity, values above zero indicate resistance. (*D*) Measurements of resistance scores are highly reproducible. Linear model: $y = f(x) = 0.96063x + 0.01916$. R^2=0.89. P <2.2E-16 (Pearson product-moment correlation, t=30.818, n=120 biological replicates). Red line, linear model; black line, diagonal with slope 1.

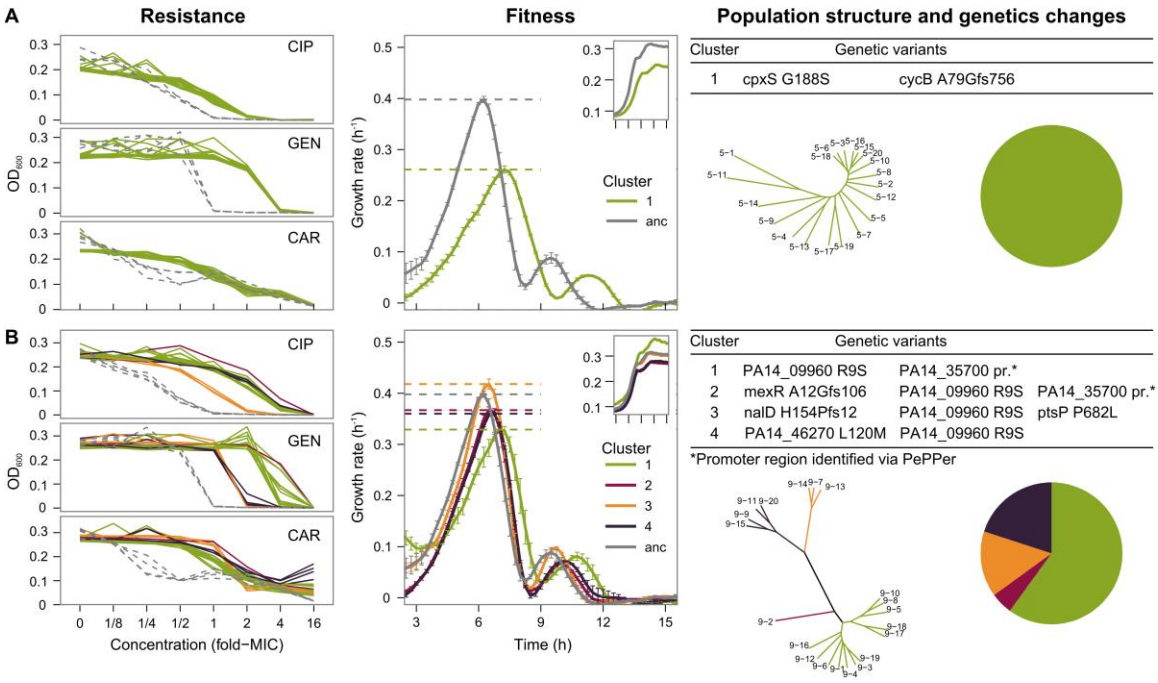

Fig. S4. Exemplary raw data of population characterization. (*A*) Population 12-1a-D8 from fast regular sequence #5. (*B*) Population 12-1b-A8 from slow regular sequence #9. Left panels show resistance measurements, as obtained by dose-response curves of 20 isolates and 4 ancestral controls. Center panel show growth rate dynamics in media without antibiotics for isolates and the ancestral strain (anc), as determined using the sliding window approach. Mean ± SEM, $n = 3$. Inlay shows growth curves. Right panels show evolved genetic changes in the tables and population structure as inferred by hierarchical clustering.

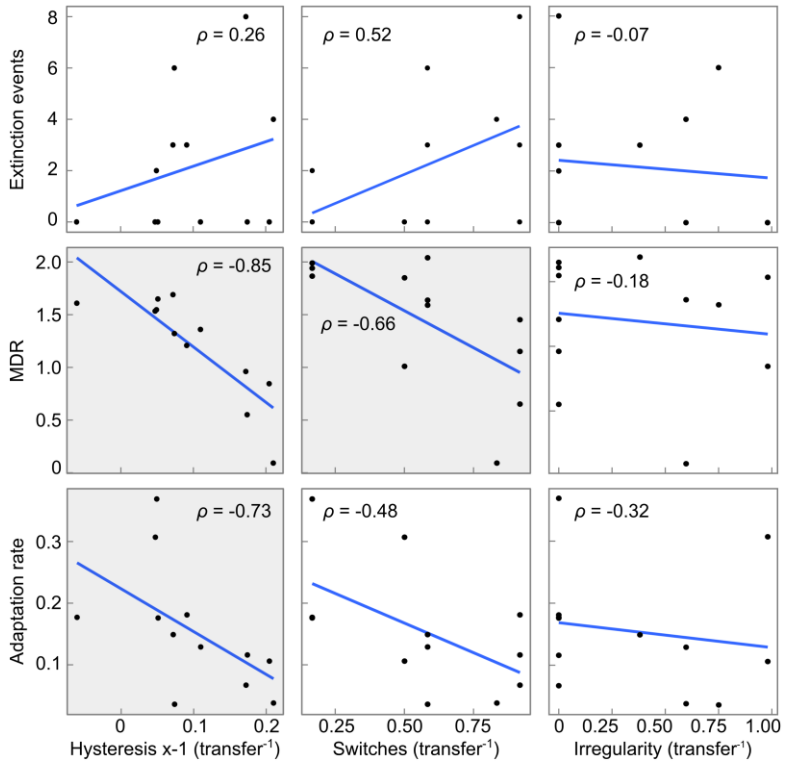

Fig. S5. Correlations of experienced hysteresis level, switching rate, and irregularity with three measures of treatment efficacy. For comparability, the correlations were restricted to all of the cycling sequences, #5-16. The major determinants of treatment efficacy are indicated across the three rows. Levels of negative hysteresis levels increase towards the right (multiplication with -1). The correlation level is indicated by the Spearman rank coefficient ρ in each of the 9 panels. Shaded plots show significant Spearman rank sum correlations.

A **Hysteresis landscape**

	CIP-> CIP	GEN-> CIP	CAR-> CIP	CIP-> GEN	GEN-> GEN	CAR-> GEN	CIP-> CAR	GEN-> CAR	CAR-> CAR
wt	1*	1.63	1.18	0.15	1	-0.36	1.09	1.15	1
CIP^R	1	1.05	1.26	0.62	1	-0.21	1.47	1.37	1
GEN^R	1	0.94	1.14	0.96	1	1.22	1.01	1.12	1
CAR^R	1	0.85	1.01	1.05	1	1.42	0.99	0.99	1

*Hysteresis factors indicating cellular sensitization or protection by previous exposure at switch of antibiotics

B **Growth rates**

	CIP 40 ng ml^{-1}	CAR 50 µg ml^{-1}	GEN 480 ng ml^{-1}
wt	0.350*	0.346	0.316
CIP^R	0.504	0.072	0.145
GEN^R	0.443	0.494	0.287
CAR^R	0.463	0.234	0.491

*Exponential growth rate

C

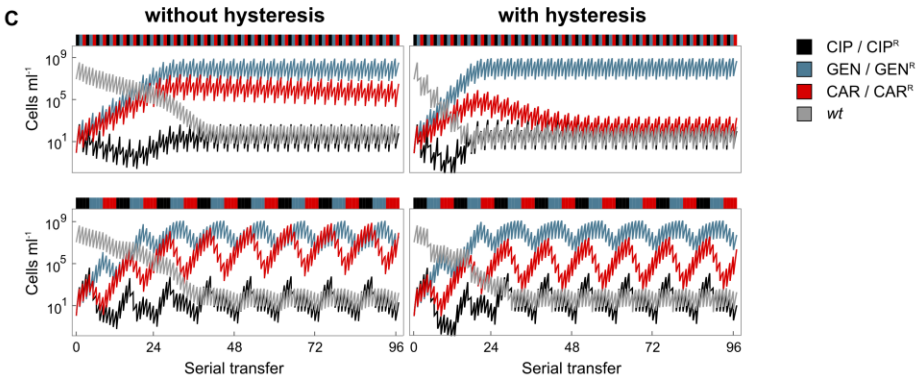

Fig. S6. Mathematical model. (*A*) Extension of hysteresis-landscape with resistant genotypes from monotherapies. Hysteresis factors for mathematical model (i.e., table *S*), as determined from time-kill experiments for evolved isolates resistant against CIP, GEN or CAR. A superscript ^{R} denotes resistance against the respective antibiotic. (*B*) Experimentally determined exponential growth rates (i.e., table *R*) during growth on antibiotics at IC_{75} concentration, for the parametrization of the model. (*C*) Modelled evolutionary growth dynamics for fast regular sequence #5 (top) and slow regular sequence #8 (bottom) as produced by a deterministic model without hysteresis or with hysteresis effects.

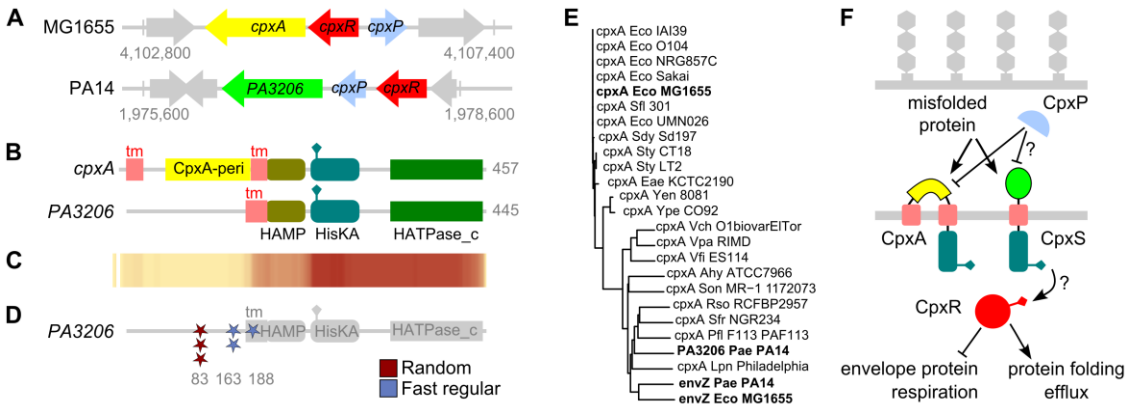

Fig. S7. Annotation of PA3206 (PA14_22730) as a new two-component sensor called cpxS. (*A*) Genomic context of *cpxA* in *E. coli* K12 MG1655 and *PA3206* (*PA14_22730*) in *P. aeruginosa* PA14, suggesting that *PA3206* may be a homolog of *cpxA*. (*B*) Protein domain structure of *E. coli* CpxA and *P. aeruginosa* PA3206. The proteins differ in length, their periplasmic sensor domain, and the number of transmembrane domains (tm). (*C*) Alignment of *E. coli* CpxA against all proteins from *P. aeruginosa* using *phmmer* shows very low coverage for the periplasmic sensor domain. (*D*) Mutational targets found in the evolved, genome-sequenced isolates are located in the putative sensor domain of *PA3206* (indicated by stars). (*E*) Phylogenetic tree of CpxA inferred from protein sequences, with protein sequences of the two-component sensor EnvZ as outgroup. (*F*) Schematic of the function and regulation of the putative two-component regulatory system CpxS/CpxR in *P. aeruginosa* in comparison to CpxA/CpxR in *E. coli*.

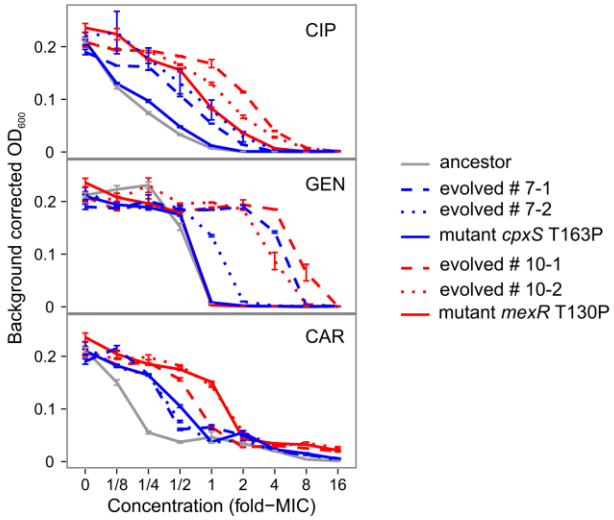

Fig. S8. Dose response curves of ancestor, evolved lineages #7-1, #7-2, #10-1, #10-2, and mutants *cpxS* T163P, *mexR* T130P as shown in Figure 5. Mean ± SEM, n = 6-20.

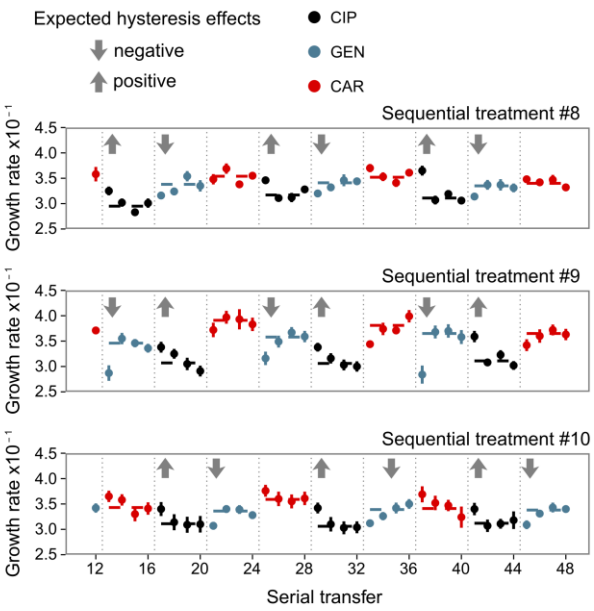

Fig. S9. Verification that cellular hysteresis effects were triggered at drug switches in the evolution experiment. Exponential growth rate of populations in slow regular protocols between transfers 12 and 48. As predicted by the hysteresis landscape in Figure 1, previous exposure to either CAR or CIP transiently inhibited growth rates on GEN (negative hysteresis, indicated by downwards arrows). The growth rates returned to baseline levels, after one transfer. Conversely, previous exposure to CAR or GEN caused transient spikes in growth rates on CIP before returning to baseline levels, which was also predicted, because previous exposures to CAR or GEN protected cells from CIP (positive hysteresis, indicated by upwards arrows). Previous exposures did not consistently affect growth rate on CAR, which agreed with hysteresis values close to zero for switches to CAR. Mean ± SEM, *n* = 10-12, extinct and putative persister population excluded.

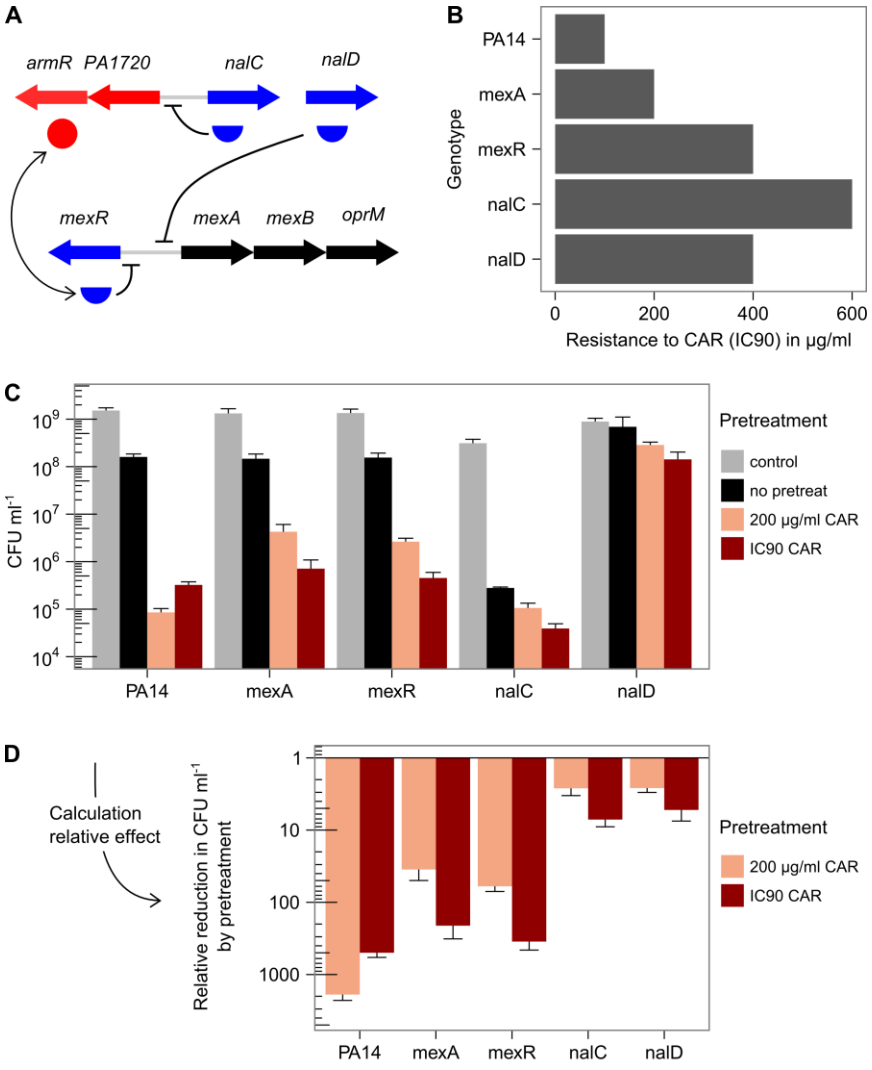

Fig. S10. Negative hysteresis in strains resistant to the antibiotic of the pretreatment. (*A*) Schematic of the regulation of the *P. aeruginosa* major multidrug efflux system MexAB-OprM, as described by Li and Plésiat (10). (*B*) Resistance of strains against CAR, as described by the concentration to inhibit visible growth after 12 h by 90% (IC_{90}). (*C*) Viable cell density (colony forming units, CFU) after treatment with 600 ng/ml GEN for 6 h (black, light red, and dark red bars), or control growth in drug-free media (gray bars). The CAR-resistant strains were either pretreated for 30 min with CAR at their respective IC_{90} (dark red bars), or with a fixed dose of 200 µg/ml CAR (light red), or received no pretreatment (black), followed by GEN treatment. Mean ± SD, n = 6 technical replicates. (*D*) Fold-reduction in viable cell density after treatment with GEN, of pretreated samples compared to samples that did not receive pretreatment, as calculated from the data in panel *C*. Mean ± SD, n = 6 technical replicates.

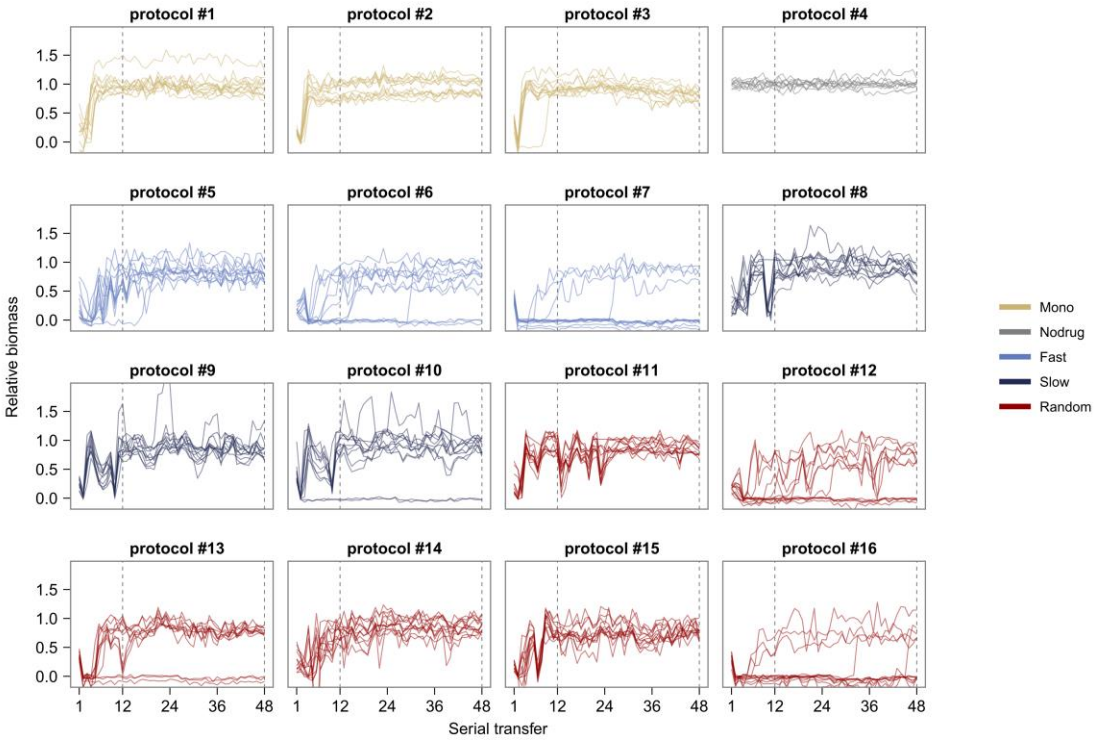

Fig. S11. Evolutionary dynamics for the 190 experimental populations. Each treatment protocol ##1-16 has 12 replicate populations, except for protocol #4, which has 10 replicates (to allow for two blank media controls for background subtraction). The different types of treatments are indicated by color (see legend on right). Extinct populations are included.

Table S1. Statistical analysis of main evolution treatments for the evolutionary dynamics shown in Figure 3*.

Comparison	Estimate	Std. error	*z*	*P*
Early phase (transfers 1-12)				
mono-fast regular	1.13413	0.10973	10.335	**<0.0001**
mono-slow regular	0.18123	0.08992	2.016	**0.0438**
mono-random	1.74299	0.16655	10.465	**<0.0001**
fast regular-slow regular	-0.9529	0.1122	-8.493	**<0.0001**
fast regular-random	-0.52527	0.21391	-2.456	**0.0169**
slow regular-random	1.38053	0.173	7.98	**<0.0001**
Middle phase (transfers 13-48)				
mono-fast regular	0.3245	0.11259	2.882	**0.007901**
mono-slow regular	0.06362	0.09168	0.694	0.58529
mono-random	0.66692	0.17155	3.888	**0.000607**
fast regular-slow regular	-0.26088	0.11437	-2.281	**0.033823**
fast regular-random	0.01792	0.21932	0.082	0.934879
slow regular-random	0.53968	0.17619	3.063	**0.006574**
Late phase (transfers 49-96)				
mono-fast regular	0.37051	0.2488	1.489	0.2729
mono-slow regular	0.03939	0.08272	0.476	0.7607
mono-random	1.07341	0.41217	2.604	0.0552
fast regular-slow regular	-0.29173	0.25141	-1.16	0.3688
fast regular-random	0.09809	0.41839	0.234	0.8146
slow regular-random	0.87646	0.42195	2.077	0.1134

* Post-hoc pairwise comparisons based on *z* statistics, following analysis of a general linear mixed model (GLMM), including relative biomass as the response variable and sequence and transfer as fixed factors and starting culture and replicate population as nested random factors. All significant *P* values are shown in bold (*P* values were corrected for multiple testing using *false discovery rate*).

Table S2. Statistical analysis of extinction frequencies using Fisher's exact tests*.

Main treatment type	Extinct	Growth		
Fast – Slow				
fast regular	11	25	***P* = 0.01201**	*odds-ratio* = 7.287493
slow regular	2	34		CI95 = 1.407, 73.282
Random – Fast				
random	11	25	*P* = 0.15	*odds-ratio* = 1.9834
fast regular	13	59		CI95 = 0.70135, 5.564
Random – Slow				
random	2	34	*P* = 0.137	*odds-ratio* = 0.2696
slow regular	13	59		CI95 = 0.0279, 1.3024

*All significant *P* values are shown in bold. The analysis refers to the data on population survival shown in Figure 2*B*.

Table S3. Statistical analysis of main evolution treatments for the inferred population diversity measurements, as shown in Figure 2*B* and Figure 3*B.**

Comparison	Estimate	Std. error	*z*	*P*
Early phase (transfers 1-12)				
mono - fast regular	0.10791	0.15178	0.711	0.596391
nodrug - fast regular	-0.05418	0.21465	-0.252	0.80072
random - fast regular	0.16393	0.13144	1.247	0.424684
slow regular - fast regular	0.79392	0.15178	5.231	**<0.0001**
nodrug - mono	-0.16209	0.21465	-0.755	0.596391
random - mono	0.05602	0.13144	0.426	0.744392
slow regular - mono	0.68601	0.15178	4.52	**<0.0001**
random - nodrug	0.21811	0.20078	1.086	0.462246
slow regular - nodrug	0.8481	0.21465	3.951	**0.000194**
slow regular - random	0.62999	0.13144	4.793	**<0.0001**

* Post-hoc pairwise comparisons based on *z* statistics, following analysis of a general linear mixed model (GLMM), including within population diversity (Shannon entropy) as the response variable and sequence as fixed factor and transfer as nested random factor. All significant *P* values are shown in bold (*P* values were corrected for multiple testing using *false discovery rate*).

Table S4. Statistical analysis of main evolution treatments for the variation in inferred multidrug resistance, shown in Figure 2 *B* and *C.**

Comparison	Estimate	Std. error	*z*	*P*
Early phase (after transfer 12)				
fast regular-slow regular	-2.0795	0.8207	-2.534	**0.0338**
fast regular-random	-1.3771	1.4462	-0.952	0.341
slow regular-random	2.7818	1.3965	1.992	0.0696
Middle phase (after transfer 48)				
fast regular-slow regular	-2.45	1.104	-2.219	0.0795
fast regular-random	-1.606	1.913	-0.84	0.4012
slow regular-random	3.294	1.913	1.722	0.1275

* Post-hoc pairwise comparisons based on *z* statistics, following analysis of a general linear mixed model (GLMM), including multidrug resistance (MDR) as the response variable and sequence as fixed factor and population as nested random factor. All significant *P* values are shown in bold (*P* values were corrected for multiple testing using *false discovery rate*).

Table S5. Fisher's exact test on the variation in *cpxS* and *mexR* mutant frequencies among distinct evolution treatments after transfer 12*.

Gene	Present	Absent		
cpxS				
fast regular	3	1	***P* = 0.02479**	*odds-ratio* = 16.67657
other	3	20		CI95 = 1.004, 1089.336
mexR				
slow regular	3	5	***P* = 0.01915**	*odds-ratio* = Inf
other	0	19		CI95 = 1.137, Inf

*All significant *P* values are shown in bold.

Table S6. Statistical analysis of replay evolution experiment, shown in Figure 4*.

Comparison	Estimate	Std. error	*z*	*P*
12rev - 12 <= 0	1.4609	0.5946	2.457	**0.014**
13 - 13rev >= 0	-0.3286	0.8258	-0.398	0.655

* Post-hoc pairwise comparisons based on *z* statistics, following analysis of a general linear mixed model (GLMM), including fold-change IC_{75} as the response variable and sequential protocol as fixed factor and antibiotic as nested random factor. All significant *P* values are shown in bold.

Table S7. Minimum duration of killing for ancestor and evolved tolerant isolate 12-1a-E2-4 (carries mutation *ispA* Y249D) from sequence #12*.

	CIP 50 ng/ml		**CAR 100 µg/ml**		**GEN 500 ng/ml**		**GEN 500 ng/ml CAR pretreated**	
	MDK_{90}	MDK_{99}	MDK_{90}	MDK_{99}	MDK_{90}	MDK_{99}	MDK_{90}	MDK_{99}
ancestor	1.23	2.81	5.37	> 6	2.69	3.46	2.05	2.65
#12 evolved	2.62	> 6	5.85	> 6	> 6	> 6	> 6	> 6

*Time in hours to kill 90% (MDK_{90}) or 99% (MDK_{99}) of the starting cell population. The corresponding time-kill data for CIP is shown in Figure 5*B*.

Movie S1. Illustration of negative hysteresis by time-lapse microscopy. Time-lapse of a time-kill experiment over 6 h using pretreatment with 100 µg/ml carbenicillin followed by exposure to 2 µg/ml gentamicin. Differential interference contrast (DIC) and corresponding fluorescence images were taken every 10 min, and composite images were assembled for the video. Dead cells are shown in red due to propidium iodide staining.

Additional data table S1 (separate file)

Genetic changes relative to the ancestral PA14 strain inferred from whole-genome resequencing. Genetic changes compared to *Pseudomonas aeruginosa* PA14 wt strain as determined by whole-genome resequencing (Illumina MiSeq2x150bp PE, Nextera libraries). Intergenic mutations are listed if they affected promoter regions, which were identified using PePPER. Isolates are coded with AA-BB-CC-DD: AA, transfer; BB, plate; CC, well; DD, colony. SEQ, sequence of antibiotics from evolution experiment; POS, position in genome; REF, allele in reference genome; ALT, alternative allele; QUAL, quality score; ST, strand; CDS, coding sequence; Na, not applicable.

Additional data table S2 (separate file)

Evolutionary trajectories of replicate populations including extinct populations. Columns: serialnumber, identifier for plate reader; plate, identifier of plate; row, row in well plate; col, column in well plate; well, well in well plate; antibiotic, antibiotic (CIP, GEN, CAR, nodrug, or empty); transfer, serial transfer number; evoexp_ID, number of treatment protocol (##1-16, empty); treatment, treatment group; line, unique name for each population; culture, starting culture; ex, extinct lineages have value 1; pers, persister lineages have value 1; auc_bg, biomass (background-corrected area under the time-OD600 growth curve); auc_rel, relative biomass (relative to evolving controls in protocol #4).

Additional data table S3 (separate file)

Resistance data for evolved isolates. Columns: transfer, serial transfer in evolution experiment after which isolates were obtained; population, unique name for population (coded AA-BB-CC: AA, transfer; BB, plate; CC, well); isolate, unique name for isolate (coded AA-BB-CC-DD: AA, transfer; BB, plate; CC, well; DD, colony); cluster, subpopulation as identified by hierarchical clustering; evoexp_ID, number of treatment protocol (##1-16); treatment, treatment group in evolution experiment; culture, starting culture; assay, identifier of assay; run, plates of the same run were measured in parallel; plate, identifier of plate; antibiotic, antibiotic (CIP, GEN, CAR); od_total, total growth (calculated from background corrected OD600), od_total_anc, total growth of ancestral reference samples measured in parallel; resistance, resistance relative to ancestor.

Additional data table S4 (separate file)

Predictors of evolutionary response for heat maps in Figure 2. Columns: category, factor that distinguishes predictors from measured responses; variable, identifier of variable; evoexp_ID, number of treatment protocol (##5-16); value, raw value; value_norm, normalized value.

Additional data table S5 (separate file)

Data from mathematical model. Columns: evoexp_ID, number of treatment protocol (##1-16); treatment, treatment group in evolution experiment; model, specifies whether the model includes

hysteresis or not (+ hys or - hys); diversity, modelled Shannon diversity; selection, modelled selection strength.

References

1. von der Schulenburg JHG, et al. (2001) Incidence of Male-Killing Rickettsia spp. (α-Proteobacteria) in the Ten-Spot Ladybird Beetle Adalia decempunctata L. (Coleoptera: Coccinellidae). *Appl Environ Microbiol* 67(1):270–277.

2. Bolger AM, Lohse M, Usadel B (2014) Trimmomatic: a flexible trimmer for Illumina sequence data. *Bioinformatics* 30(15):2114–2120.

3. Winsor GL, et al. (2016) Enhanced annotations and features for comparing thousands of Pseudomonas genomes in the Pseudomonas genome database. *Nucleic Acids Res* 44(Database issue):D646–D653.

4. Langmead B, Salzberg SL (2012) Fast gapped-read alignment with Bowtie 2. *Nat Methods* 9(4):357–359.

5. Li H, et al. (2009) The Sequence Alignment/Map format and SAMtools. *Bioinforma Oxf Engl* 25(16):2078–2079.

6. Danecek P, et al. (2011) The variant call format and VCFtools. *Bioinformatics* 27(15):2156–2158.

7. Barbosa C, et al. (2017) Alternative Evolutionary Paths to Bacterial Antibiotic Resistance Cause Distinct Collateral Effects. *Mol Biol Evol* 34(9):2229–2244.

8. de Jong A, Pietersma H, Cordes M, Kuipers OP, Kok J (2012) PePPER: a webserver for prediction of prokaryote promoter elements and regulons. *BMC Genomics* 13:299.

9. Trebosc V, et al. (2016) A Novel Genome-Editing Platform for Drug-Resistant Acinetobacter baumannii Reveals an AdeR-Unrelated Tigecycline Resistance Mechanism. *Antimicrob Agents Chemother* 60(12):7263–7271.

10. Li X-Z, Plésiat P (2016) Antimicrobial Drug Efflux Pumps in Pseudomonas aeruginosa. *Efflux-Mediated Antimicrobial Resistance in Bacteria: Mechanisms, Regulation and Clinical Implications*, eds Li X-Z, Elkins CA, Zgurskaya HI (Adis, New York, NY), pp 359–400. 1st ed. 2016 edition.